


# Optical properties of five-layer and ten-layer $CrI_3$ films under high pressure: Insights from *in situ* Raman and UV–visible spectroscopy

Zhipeng Yan(闫志鹏), Xiaodong Yao(姚晓东), Guangyang Dai(代光阳), Chenkai Li(李辰恺), Qunfei Zheng(郑群飞), Jun Han(韩军), Ying Liu(刘影), and Xiaowei Sun(孙小伟)

**Citation:**Chin. Phys. B, 2026, 35 (**5**): 057801. DOI: 10.1088/1674-1056/ae40d9
http://cpb.iphy.ac.cn; http://iopscience.iop.org/cpb

**What follows is a list of articles you may be interested in**

---

## Stokes/anti-Stokes Raman spectroscopy of $Al_{0.86}Ga_{0.14}N$ semiconductor alloy

Yuru Lin(林玉茹), Yu Li(李宇), Binbin Wu(吴彬彬), Jingyi Liu(刘静仪), Ruiang Guo(郭睿昂), Yangbin Wang(王扬斌), Qiwei Hu(胡启威), and Li Lei(雷力)

Chin. Phys. B, 2025, 34 (**5**): 057802. DOI: 10.1088/1674-1056/adb67d

## Intensity enhancement of Raman active and forbidden modes induced by naturally occurred hot spot at GaAs edge

Tao Liu(刘涛), Miao-Ling Lin(林妙玲), Da Meng(孟达), Xin Cong(从鑫), Qiang Kan(阚强), Jiang-Bin Wu(吴江滨), and Ping-Heng Tan(谭平恒)

Chin. Phys. B, 2025, 34 (**1**): 017801. DOI: 10.1088/1674-1056/ad9ff9

## Identifying the effect of photo-generated carriers on the phonons in rutile $TiO_2$ through Raman spectroscopy

Zheng Wang(王征), Min Liao(廖敏), Guihua Wang(王桂花), and Meng Zhang(张梦)

Chin. Phys. B, 2024, 33 (**11**): 117802. DOI: 10.1088/1674-1056/ad73b4

## Unveiling localized electronic properties of $ReS_2$ thin layers at nanoscale using Kelvin force probe microscopy combined with tip-enhanced Raman spectroscopy

Yu Luo(罗宇), Weitao Su(苏伟涛), Juanjuan Zhang(张娟娟), Fei Chen(陈飞), Ke Wu(武可), Yijie Zeng(曾宜杰), and Hongwei Lu(卢红伟)

Chin. Phys. B, 2023, 32 (**11**): 117801. DOI: 10.1088/1674-1056/ace425

## Signal-to-noise ratio of Raman signal measured by multichannel detectors

Xue-Lu Liu(刘雪璐), Yu-Chen Leng(冷宇辰), Miao-Ling Lin(林妙玲), Xin Cong(从鑫), and Ping-Heng Tan(谭平恒)

Chin. Phys. B, 2021, 30 (**9**): 097807. DOI: 10.1088/1674-1056/ac1f06

---

**SPECIAL TOPIC — Structures and properties of materials under high pressure**

# Optical properties of five-layer and ten-layer $CrI_3$ films under high pressure: Insights from *in situ* Raman and UV–visible spectroscopy

Zhipeng Yan(闫志鹏)[1,2,†], Xiaodong Yao(姚晓东)[3], Guangyang Dai(代光阳)[2,4], Chenkai Li(李辰恺)[3], Qunfei Zheng(郑群飞)[3], Jun Han(韩军)[3], Ying Liu(刘影)[3], and Xiaowei Sun(孙小伟)[1,‡]

[1] *School of Mathematics and Physics, Lanzhou Jiaotong University, Lanzhou* 730070, *China*
[2] *Academy for Advanced Interdisciplinary Studies, Southern University of Science and Technology, Shenzhen* 518055, *China*
[3] *Department of Physics, Southern University of Science and Technology, Shenzhen* 518055, *China*
[4] *Institute of Quantum Materials and Physics, Henan Academy of Sciences, Zhengzhou* 450046, *China*

(Received 6 November 2025; revised manuscript received 14 January 2026; accepted manuscript online 3 February 2026)

The two-dimensional van der Waals ferromagnetic semiconductor $CrI_3$ provides an ideal platform for exploring the interplay among structural, electronic and magnetic degrees of freedom. In this work, we systematically investigate the thickness-dependent optical properties of five-layer and ten-layer $CrI_3$ under hydrostatic pressure up to 27.9 GPa by *in situ* Raman and UV–visible absorption spectroscopy. All $A_g$ Raman modes exhibit a continuous blueshift with increasing pressure. The low-frequency modes ($A_g^1 - A_g^3$) are mainly associated with enhanced interlayer coupling, whereas the high-frequency modes ($A_g^4 - A_g^6$) reflect the suppression of surface vibrations. The Raman modes disappear at approximately 4.9 GPa for the five-layer sample and 11.2 GPa for the ten-layer sample, indicating a stronger strain sensitivity in thinner $CrI_3$. Optical absorption measurements show a pronounced redshift of the absorption edge, accompanied by bandgap narrowing from 2.26 eV to 1.26 eV in five-layer $CrI_3$. At comparable pressures, the five-layer sample consistently exhibits a wider bandgap than the ten-layer one, which is attributed to quantum confinement effects and reduced interlayer hybridization. Above 12.7 GPa, the bandgap reduction becomes less pronounced, probably due to enhanced Cr 3d/I 5p orbital overlap and strengthened superexchange interactions. These results reveal a clear layer-dependent structure–electronic coupling in $CrI_3$ under compression and provide useful insights into pressure modulation of van der Waals magnetic semiconductors.

**Keywords:** a few layered $CrI_3$, Raman spectroscopy, UV–vis absorption spectrum, high pressure

**PACS:** 78.30.–j, 63.22.–m, 78.20.–e, 78.66.–w

**DOI:** 10.1088/1674-1056/ae40d9 **CSTR:** 32038.14.CPB.ae40d9

## 1. Introduction

Two-dimensional van der Waals (vdW) magnetic materials have emerged as a novel platform for quantum materials research since the discovery of intrinsic ferromagnetism in monolayer $CrI_3$ in 2017, and have rapidly attracted extensive attention in condensed matter physics and spintronics.[1–3] Owing to their atomic-scale thickness, weak interlayer vdW bonding and tunable magnetic ordering, these materials transcend the dimensional limitations of conventional three-dimensional magnets, exhibiting exotic magnetic phenomena and promising potential for device applications.[4–7] As a prototypical vdW magnet, $CrI_3$ consists of a honeycomb lattice of $Cr^{3+}$ ions, where ferromagnetic coupling is mediated by Cr–I–Cr superexchange pathways with near 90° bond angles, giving rise to a Curie temperature ($T_C$) of approximately 61 K in the bulk form.[1,8] Notably, the magnetic properties of $CrI_3$ are highly sensitive to layer number, stacking configuration and external perturbations such as pressure, magnetic field and strain, making it an ideal model system for investigating the evolution of magnetism in reduced dimensions.[9–11]

$CrI_3$ crystallizes in a layered vdW structure composed of edge-sharing $CrI_6$ octahedra, with adjacent layers coupled via weak vdW interactions. Bulk $CrI_3$ adopts a monoclinic stacking structure (space group $C2/m$) at room temperature and undergoes a structural transition to a rhombohedral phase (space group $R\bar{3}$) below approximately 220 K.[12–15] This stacking transition has a profound impact on the interlayer magnetic coupling: the rhombohedral phase favors ferromagnetic (FM) interlayer exchange, whereas the monoclinic phase stabilizes antiferromagnetic (AFM) interlayer coupling.[16,17] In few-layer $CrI_3$, monoclinic stacking dominates, leading to AFM order in bilayers ($T_M \approx 45$ K) and FM order in odd-layered samples.[10,18] This layer-parity-dependent magnetic behavior is closely related to the Mermin–Wagner theorem for two-dimensional isotropic Heisenberg systems, which requires magnetocrystalline anisotropy to stabilize long-range

†Corresponding author. E-mail: zp.yan@lzjtu.edu.cn
‡Corresponding author. E-mail: sunxw_lzjtu@yeah.net

© 2026 Chinese Physical Society and IOP Publishing Ltd. All rights, including for text and data mining, AI training, and similar technologies, are reserved.

magnetic order.[19–21]

Hydrostatic pressure serves as an effective non-chemical tuning parameter that compresses interlayer spacing, modifies bond angles and alters lattice symmetry, thereby strongly influencing the magneto-electronic properties of $CrI_3$. Experimental and theoretical studies on bulk single-crystalline $CrI_3$ have shown that moderate pressure ($< 3$ GPa) enhances FM exchange interactions and increases $T_C$ to approximately 66 K by driving the Cr–I–Cr bond angle closer to 90°. In contrast, further compression ($> 10$ GPa) leads to a rapid suppression of ferromagnetism, with $T_C$ decreasing to $\sim 10$ K near 21 GPa, accompanied by magnetic instability and the emergence of complex or AFM spin configurations.[22,23] This pressure-induced magnetic transition is attributed to excessive bond-angle compression (to $\sim 85°$), which weakens FM superexchange and introduces competing AFM interactions. Meanwhile, $CrI_3$ undergoes a pressure-driven semiconductor-to-metal transition, as confirmed by resistivity measurements and density functional theory calculations which reveal bandgap closure.[22] These findings not only elucidate the microscopic mechanisms of magnetostructural coupling but also shed light on the origin of topological spin excitations. Inelastic neutron scattering experiments demonstrate that the acoustic–optical spin-wave gap at the Dirac point is dominated by next-nearest-neighbor Dzyaloshinskii–Moriya interactions rather than Kitaev exchange or electron correlation effects. External magnetic fields further tune these excitations, confirming the presence of $c$-axis nearest-neighbor AFM and next-nearest-neighbor FM interactions.[24,25]

In few-layer $CrI_3$, pressure tuning becomes even more intricate. Raman spectroscopy studies reveal that the $E_g$ modes in one- to four-layer $CrI_3$ split into $A_g$ and $B_g$ modes with increasing thickness, with the mode separation saturating in thicker samples. Upon cooling to 10 K, these modes tend to merge but do not fully recover rhombohedral stacking, indicating the persistence of surface-layer monoclinic distortions.[26,27] Experiments on trilayer $CrI_3$ have identified three distinct magnetic configurations (FM-↑↑↑, FM-↓↑↓ and FM-↑↑↓), which are theoretically attributed to subtle tensile strains associated with different stacking orders, including rhombohedral, monoclinic, hexagonal and triclinic structures.[9,28] Such strain effects effectively mimic pressure-induced modifications of interlayer coupling and $T_C$. Moreover, vdW heterostructures, such as $CrI_3/CrBr_3$, further amplify pressure effects, where threshold pressures can induce AFM–FM switching, accompanied by dramatic variations in magnetic anisotropy energy depending on interface bonding and spin orientation.[29,30]

Despite these advances, most existing studies remain theoretical, and experimental investigations of few-layer $CrI_3$ under high pressure are still scarce. In this work, we systematically investigate the structural and optical responses of five-layer and ten-layer $CrI_3$ under high pressure. Our results reveal a series of pressure-induced structural evolutions and bandgap modifications. Raman spectroscopy demonstrates that the five-layer sample exhibits significantly stronger pressure sensitivity than the ten-layer sample, while UV–visible absorption measurements show that the bandgap of five-layer $CrI_3$ remains consistently larger under the same pressure conditions. These findings elucidate the thickness-dependent structure–electronic coupling in $CrI_3$ under compression and provide valuable insights for the engineering of vdW magnetic materials.

## 2. Experimental methods

Commercial single-crystal $CrI_3$ samples were used to prepare thin-layer specimens. The bulk crystals were mechanically exfoliated into thin flakes using Scotch tape and subsequently inspected under an optical microscope. Flakes with different thicknesses were preliminarily identified based on optical contrast and further confirmed by atomic force microscopy (AFM), as shown in supplementary material Fig. S1. High-quality five-layer and ten-layer $CrI_3$ samples were selected for subsequent measurements. The selected flakes were transferred onto diamond anvils by a dry-transfer method using polydimethylsiloxane; the detailed transfer procedures are illustrated in supplementary material Fig. S2. All exfoliation and transfer processes were carried out in a nitrogen-filled glovebox to minimize sample degradation. Symmetric diamond anvil cells (DACs) were employed to generate hydrostatic pressure conditions. A T301 stainless-steel gasket was pre-indented to a thickness of approximately 30 μm, and a sample chamber with a diameter of about 140 μm was drilled at the center of the gasket. *In situ* high-pressure measurements were performed using the DAC, with pressure calibrated by the ruby fluorescence method. Silicone oil was used as the pressure-transmitting medium (PTM) for both Raman spectroscopy and UV–visible absorption measurements.[31,32] Raman spectra were collected using a solid-state laser with a Nd:YAG crystal ($\lambda = 532$ nm) and a liquid-nitrogen-cooled charge-coupled device detector, providing a spectral resolution better than 1 $cm^{-1}$. UV–visible absorption spectroscopy was carried out over a wavelength range of 250–1000 nm.

## 3. Results and discussion

### 3.1. Raman spectroscopy measurements

The DAC technique, combined with a hydrostatic PTM, provides an effective approach for probing the vibrational and structural properties of layered $CrI_3$, as illustrated in Fig. 1(a). Thin-layer $CrI_3$ samples were obtained by mechanical exfoli-

ation, and the layer number was initially identified using optical contrast analysis. In the high-temperature phase of $CrI_3$, each layer adopts a honeycomb lattice of Cr atoms, where each Cr atom is octahedrally coordinated by six I atoms. In the monoclinic phase, adjacent layers are laterally displaced by a translation vector of (1/3, 0), as schematically shown in Fig. 1(b). Such structural variations can be effectively characterized by polarized Raman spectroscopy. Figure 1(c) displays optical micrographs of the five-layer and ten-layer $CrI_3$ flakes immersed in the PTM inside the DAC. The corresponding Raman spectra are presented in Fig. 1(d), which further confirm the assigned layer numbers.

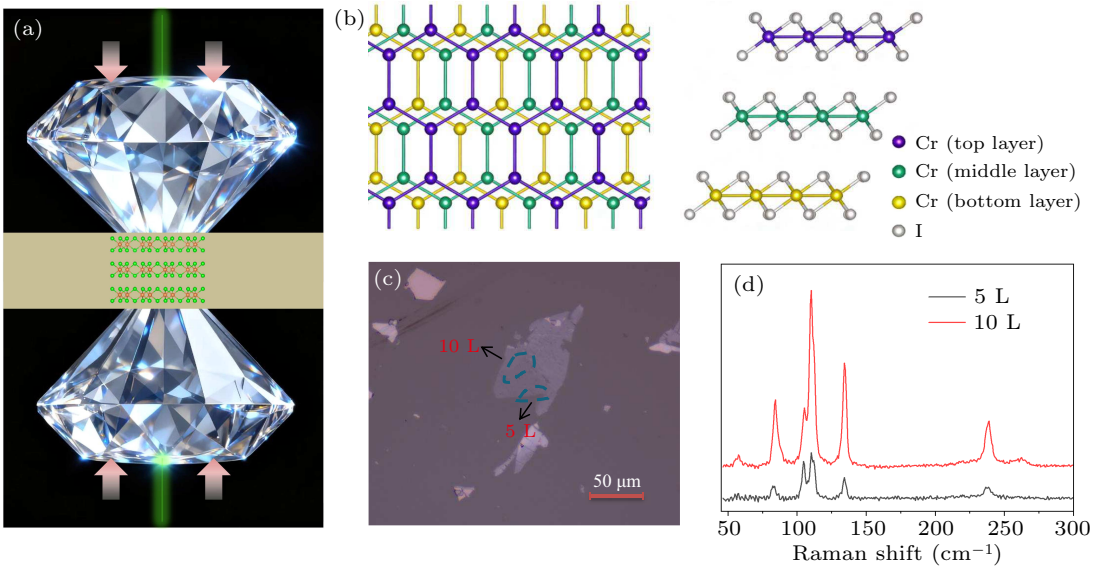



**Fig. 1.** The effect of pressure on the optical properties of five-layer and ten-layer $CrI_3$ was investigated. (a) Schematic diagram of the experimental setup for crystal structure manipulation of five-layer and ten-layer $CrI_3$ using a diamond anvil cell. (b) Top and side views of monoclinic $CrI_3$. (c) Optical photographs of the five-layer and ten-layer $CrI_3$ samples used in this study. (d) Raman spectroscopy confirms the five-layer and ten-layer samples.

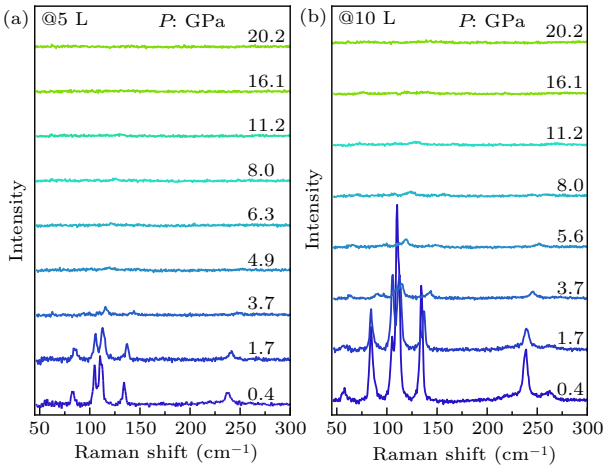



**Fig. 2.** Selected Raman spectra of (a) five and (b) ten layers of $CrI_3$ under high pressure.

Raman spectroscopy was employed to investigate the pressure-dependent vibrational properties of five-layer and ten-layer $CrI_3$. Figures 2(a) and 2(b) present the Raman spectra of the two samples with different thicknesses measured at various pressures. For the five-layer $CrI_3$ sample (Fig. 2(a)), the Raman signal intensity decreases rapidly with increasing pressure and becomes extremely weak above 4.9 GPa. When the pressure exceeds approximately 6.3 GPa, the signal-to-noise ratio of all observed features drops below $\sim 2$, and the remaining spectral features are comparable to the background noise. Under these conditions, the Raman signals can no longer be reliably assigned to specific phonon modes. In contrast, the ten-layer $CrI_3$ sample (Fig. 2(b)) exhibits discernible Raman peaks up to 11.2 GPa, with the peaks gradually weakening at higher pressures. The Raman modes persist until the pressure exceeds 16.2 GPa, beyond which they vanish completely. A direct comparison of the *in situ* high-pressure Raman spectra demonstrates that the disappearance of Raman modes in the ten-layer sample is delayed by more than 10 GPa relative to the five-layer sample, indicating a significantly enhanced pressure tolerance with increasing thickness. In addition, a Raman mode at approximately 57.5 cm$^{-1}$ is observed exclusively in the ten-layer $CrI_3$ and is absent in the five-layer sample, suggesting that the vibrational characteristics of the thicker sample more closely resemble those of bulk $CrI_3$.

Based on group-theoretical analysis of the $\Gamma$-point lattice vibrations in $CrI_3$, the Raman-active phonon modes can be classified into two irreducible representations, $A_g$ and $B_g$. The $A_g$ modes correspond to interlayer symmetric stretching and bending vibrations, such as uniform Cr–I bond stretching or interlayer symmetric breathing motions. These modes are highly sensitive to interlayer coupling and are therefore widely employed as probes of stacking order. In contrast, the $B_g$ modes represent antisymmetric vibrations, which are odd under the $C_2$ operation and even under inversion symmetry,

and are associated with shear or asymmetric stretching motions, including interlayer sliding and relative Cr–I bond displacements. Owing to their symmetry, these modes are more susceptible to magnetic effects, particularly spin–phonon coupling. Figure 3(a) shows the pressure-induced blueshift of the $A_g$ modes for both five-layer and ten-layer $CrI_3$ samples. To further elucidate thickness-dependent vibrational behavior, we quantitatively compared the frequency differences between the two samples for the lower-frequency modes ($A_g^1 - A_g^3$) and higher-frequency modes ($A_g^4 - A_g^6$) as a function of pressure, as shown in Fig. 3(b). Below 3 GPa, the frequency differences associated with the interlayer symmetric breathing mode ($A_g^1$), the Cr–I symmetric bending mode ($A_g^2$), and the Cr–I symmetric stretching mode ($A_g^3$) exhibit oscillatory behavior. In contrast, for the in-plane bending mode ($A_g^4$), the Cr–I stretching mode ($A_g^5$) and the higher-frequency symmetric stretching mode ($A_g^6$), the frequency differences gradually increase in this pressure range. When the pressure exceeds 3 GPa, the frequency differences of the $A_g^1 - A_g^3$ modes between the five-layer and ten-layer samples progressively widen, whereas those of the $A_g^4 - A_g^6$ modes gradually decrease. These contrasting trends indicate that, in few-layer $CrI_3$, the $A_g^1 - A_g^3$ "soft" modes predominantly reflect interlayer coupling effects, which are more strongly enhanced in the thinner (five-layer) sample under pressure. In contrast, the high-frequency $A_g^4 - A_g^6$ "hard" modes are primarily associated with surface-related vibrations, whose layer dependence is progressively weakened under compression, leading to their more uniform suppression. These observations provide useful insights into the pressure-dependent vibrational behavior of few-layer $CrI_3$ and the findings may be extended to other two-dimensional layered materials.

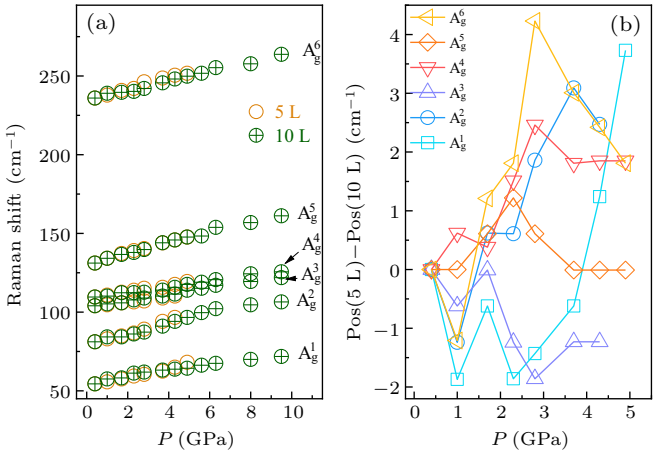



**Fig. 3.** (a) Raman modes of five-layer and ten-layer $CrI_3$ as a function of pressure. (b) The difference in Raman modes between five-layer and ten-layer $CrI_3$ under the same pressure as a function of pressure.

### 3.2. Ultraviolet–visible absorption spectroscopy measurements

As a layered vdW ferromagnetic semiconductor, investigating the optical bandgap of two-dimensional $CrI_3$ not only provides insight into the coupling between its electronic structure and magnetic ordering but also offers important implications for potential spintronic and optoelectronic applications. To this end, UV–visible absorption spectroscopy was employed to examine the pressure-dependent evolution of the direct optical bandgap in five-layer and ten-layer $CrI_3$, as shown in Figs. 4(a) and 4(b). With increasing pressure, the absorption edges of both samples gradually shift toward lower photon energies, accompanied by a pronounced suppression of absorption features, indicating continuous bandgap narrowing. When the pressure exceeds 7 GPa, the absorption peaks in the five-layer $CrI_3$ sample disappear, whereas those in the ten-layer sample vanish at a lower pressure of approximately 4.4 GPa, reflecting distinct thickness-dependent responses to compression. In $CrI_3$, the $Cr^{3+}$ ions adopt a $d^3$ electronic configuration in an octahedral $CrI_6$ coordination environment, giving rise to characteristic intra-atomic d–d transitions. Among these, the $^4A_2 \rightarrow {}^4T_2$ transition corresponds to the lowest-energy d–d excitation. A comparison of the pressure evolution of these transitions reveals that the d–d absorption features in the ten-layer sample are suppressed at lower pressures than those in the five-layer sample. The pressure dependence of the optical bandgap for both samples, extracted using the Tauc method, is summarized in Fig. 4(c) (details of the data fitting are given in the supplementary material Fig. SI3). At a given pressure, the optical bandgap of the five-layer $CrI_3$ remains consistently larger than that of the ten-layer sample, which can be attributed to a combination of quantum confinement effects, reduced interlayer coupling and variations in magnetic ordering. Notably, when the pressure exceeds approximately 12.7 GPa, the rate of bandgap narrowing with increasing pressure becomes markedly reduced. This behavior suggests that at higher pressures, enhanced lattice compression increases the overlap between Cr 3d and I 5p orbitals, leading to modifications of both the conduction band minimum (CBM) and the valence band maximum (VBM). Meanwhile, strengthened superexchange interactions may further influence the electronic structure, collectively contributing to the observed slowdown in bandgap reduction.

The Raman spectroscopy results provide detailed insight into the pressure-induced structural and vibrational evolution of few-layer $CrI_3$, highlighting the interplay between interlayer coupling and surface effects in thickness-dependent systems. Under hydrostatic pressure, both five-layer and ten-layer samples exhibit systematic blueshifts of the $A_g$ modes, indicating lattice stiffening driven by Cr–I bond compression and reduced interlayer spacing, which collectively enhance bonding strength. A pronounced thickness dependence is observed in the critical pressure at which Raman modes disappear, occurring at approximately 4.9 GPa for the five-layer sample and 11.2 GPa for the ten-layer sample. This $\sim 6$ GPa difference

underscores the crucial role of thickness in pressure modulation: thinner samples, characterized by larger surface-to-volume ratios, are more susceptible to nonuniform strain accumulation under compression, which accelerates vibrational disorder and structural instability. The critical pressure for Raman peak disappearance — indicative of structural disordering or amorphization rather than a semiconductor–metal transition — differs markedly between thicknesses: 4.9 GPa for five-layer $CrI_3$ (with peaks fully vanishing by 6.3 GPa) and 11.2 GPa for ten-layer $CrI_3$ (persisting until 16.2 GPa). This disappearance, quantified as mode intensity dropping below 10% of ambient with signal-to-noise ratio $< 2$, is likely to stem from pressure-driven loss of long-range crystalline order, where compressed interlayer spacing and Cr–I bond distortions lead to phonon broadening and quenching. In addition, the Raman mode at $\sim 57.5$ cm$^{-1}$ observed exclusively in the ten-layer $CrI_3$ can be attributed to bulk-like interlayer shear vibrations, which are absent in thinner samples due to weakened vdW coupling. These observations are further clarified through group-theoretical analysis. $A_g$ modes, associated with symmetric stretching and bending vibrations, serve as sensitive probes of interlayer symmetry, whereas $B_g$ modes correspond to antisymmetric shear motions and are more susceptible to magnetic perturbations. $A_g^1 - A_g^3$ modes (50–130 cm$^{-1}$) exhibit oscillatory frequency differences below 3 GPa, reflecting dynamic adjustments in weak interlayer coupling, reminiscent of phonon softening phenomena in strained vdW heterostructures. Above 3 GPa, the frequency differences of the $A_g^1 - A_g^3$ modes progressively increase, indicating enhanced interlayer coupling, whereas those of the $A_g^4 - A_g^6$ modes decrease, suggesting a gradual suppression of surface-related vibrations as pressure homogenizes internal strain fields. This layer-dependent dichotomy is consistent with previous reports on few-layer $CrI_3$, where surface monoclinic distortions persist and delay the rhombohedral transition at low temperatures.[26,33] Our results extend this picture to the high-pressure regime, implying that thinner $CrI_3$ layers effectively act as "pressure amplifiers," with interlayer breathing modes ($A_g^1$) promoting accelerated structural instabilities under compression.

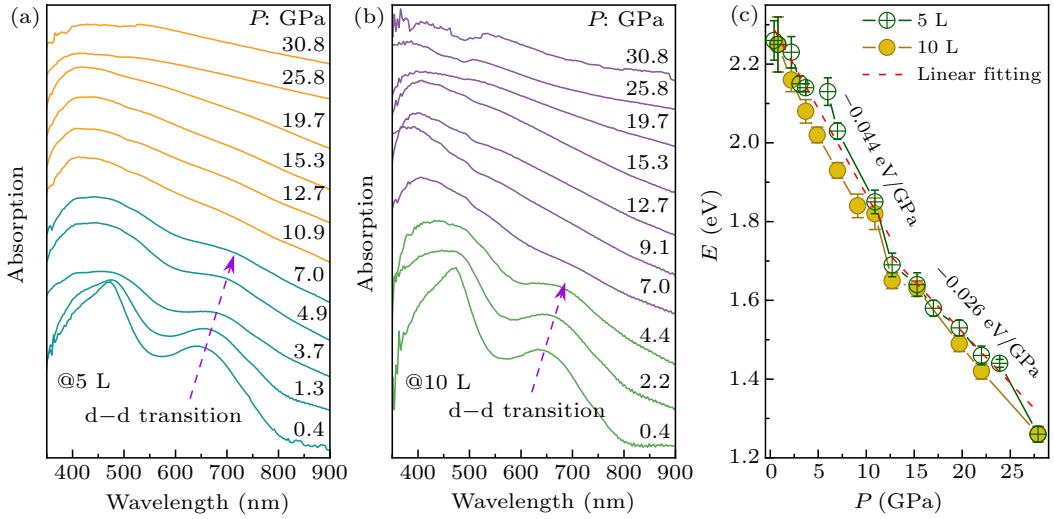



**Fig. 4.** Selected optical absorption spectra of (a) five and (b) ten layers of $CrI_3$ under high pressure. (c) Bandgap evolution of five and ten layers of $CrI_3$ up to 27.9 GPa.

Complementary UV–visible absorption measurements further elucidate the pressure-induced electronic bandgap renormalization in few-layer $CrI_3$. With increasing pressure, the absorption edges shift systematically toward lower photon energies, reflecting the continuous narrowing of the optical bandgap. For the five-layer sample, the bandgap decreases from approximately 1.8 eV at ambient pressure to $\sim 1.4$ eV at 7 GPa, while a similar trend is observed in the ten-layer sample, albeit with an earlier suppression of absorption features above $\sim 4.4$ GPa. Notably, at equivalent pressures, the five-layer $CrI_3$ consistently retains a larger bandgap by approximately 0.1 eV, which can be attributed to quantum confinement effects and reduced interlayer hybridization, in agreement with density functional theory predictions of spin-polarized bandgaps in $CrI_3$.[34,35] The optical response is dominated by intra-atomic d–d transitions of $Cr^{3+}$ ions in the octahedral $CrI_6$ environment, with the lowest-energy transition corresponding to the $^4A_2 \rightarrow {}^4T_2$ excitation in the 1.6–2.0 eV range. Pressure suppresses this transition at lower pressures in the thicker sample, possibly due to enhanced lattice distortions under bulk-like compression. At higher pressures, lattice contraction increases Cr 3d–I 5p orbital overlap and strengthens superexchange interactions, moderating further bandgap reduction. The enhanced pressure tolerance of excitonic features in thinner samples suggests a higher resilience of spin-dependent optical responses, which may be advantageous for magneto-optical and spin-valley applications in vdW magnetic semiconductors.[36] Overall, these results establish a clear cor-

relation between thickness, pressure response and structure–electronic coupling in few-layer $CrI_3$, providing experimental guidance for pressure engineering of two-dimensional vdW magnets.

## 4. Conclusion

In summary, we have systematically investigated the thickness-dependent optical properties of five-layer and ten-layer $CrI_3$ using *in situ* high-pressure Raman and UV–visible absorption spectroscopy. Our results show that all $A_g$ Raman modes exhibit continuous blueshifts with increasing pressure. The $A_g^1 - A_g^3$ modes reflect enhanced interlayer coupling, whereas the $A_g^4 - A_g^6$ modes indicate progressive suppression of surface-related vibrations. The Raman modes disappear at approximately 4.9 GPa in the five-layer $CrI_3$ and persist up to about 11.2 GPa in the ten-layer sample, demonstrating a markedly stronger pressure sensitivity in thinner layers. This behavior is attributed to enhanced quantum confinement and pronounced surface-induced strain gradients. Optical absorption measurements reveal a pressure-induced redshift of the absorption edge, corresponding to significant bandgap narrowing from 2.26 eV to 1.26 eV in the five-layer sample. At comparable pressures, the five-layer $CrI_3$ consistently maintains a larger bandgap than the ten-layer counterpart, owing to reduced interlayer hybridization and the suppression of the $Cr^{3+}$ d–d transition ($^4A_2 \rightarrow {}^4T_2$). Notably, when the pressure exceeds approximately 12.7 GPa, the rate of bandgap reduction decreases substantially, which can be associated with enhanced Cr 3d–I 5p orbital overlap and strengthened superexchange interactions. Overall, these findings elucidate the layer-dependent structure–electronic coupling mechanisms of $CrI_3$ under high pressure and provide valuable physical insights for pressure modulation of vdW magnetic semiconductors.

## Acknowledgements

This work was mainly supported by the National Natural Science Foundation of China (Grant No. 12274193) and Natural Science Foundation of Henan (Grant No. 242300420640). We also thank the support from Tianyou Youth Talent Lift Program of Lanzhou Jiaotong University and the Young Scholars Science Foundation of Lanzhou Jiaotong University (Grant No. 2025027).

## References

[1] Huang B, Clark G, Navarro-Moratalla E, Klein D R, Cheng R, *et al* 2017 *Nature* **546** 270
[2] Lado J L and Fernández-Rossier J 2017 *2D Mater.* **4** 035002
[3] Wang X, Wang C, Wang Y, Ye C, Rahman A, *et al* 2025 *ACS Nano* **19** 8108
[4] Gong C, Li L, Li Z, Ji H, Stern A, *et al* 2017 *Nature* **546** 265
[5] Deng Y, Yu Y, Song Y, Zhang J, Wang N Z, *et al* 2018 *Nature* **563** 94
[6] Deng Y, Yu Y, Shi M Z, Guo Z, Xu Z, *et al* 2020 *Science* **367** 895
[7] Xiao F and Tong Q 2022 *Nano Lett.* **22** 3946
[8] Webster L and Yan J A 2018 *Phys. Rev. B* **98** 144411
[9] Song T, Fei Z, Yankowitz M, Lin Z, Jiang Q, *et al* 2019 *Nat. Mater.* **18** 1298
[10] Sivadas N, Okamoto S, Xu X, Fennie C J and Xiao D 2018 *Nano Lett.* **18** 7658
[11] Wu Z, Yu J and Yuan S 2019 *Phys. Chem. Chem. Phys.* **21** 7750
[12] McGuire M A, Dixit H, Cooper V R and Sales B C 2015 *Chemistry of Materials* **27** 612
[13] Tomarchio L, Macis S, Mosesso L, Nguyen L T, Grilli A, *et al* 2021 *Sci. Rep.* **11** 23405
[14] Dillon J F, Jr. and Olson C E 1965 *J. Appl. Phys.* **36** 1259
[15] Meseguer-Sánchez J, Popescu C, García-Muñoz J L, Luetkens H, Taniashvili G, *et al* 2021 *Nat. Commun.* **12** 6265
[16] Li T, Jiang S, Sivadas N, Wang Z, Xu Y, *et al* 2019 *Nat. Mater.* **18** 1303
[17] Jiang Y, Guo Y, Yan X, Zeng H, Lin L, *et al*. 2021 *Nanomaterials* **11** 2509
[18] Jiang S, Li L, Wang Z, Mak K F and Shan J 2018 *Nature Nanotechnology* **13** 549
[19] Mermin N D and Wagner H 1966 *Phys. Rev. Lett.* **17** 1133
[20] Hohenberg P C 1967 *Phys. Rev.* **158** 383
[21] Burch K S, Mandrus D and Park J G 2018 *Nature* **563** 47
[22] Ghosh A, Singh D, Aramaki T, Mu Q, Borisov V, *et al*. 2022 *Phys. Rev. B* **105** L081104
[23] Mondal S, Kannan M, Das M, Govindaraj L, Singha R, *et al* 2019 *Phys. Rev. B* **99** 180407
[24] Chen L, Chung J-H, Gao B, Chen T, Stone M B, *et al* 2018 *Phys. Rev. X* **8** 041028
[25] Chen L, Chung J-H, Stone M B, Kolesnikov A I, Winn B, *et al* 2021 *Phys. Rev. X* **11** 031047
[26] Guo X, Jin W, Ye Z, Ye G, Xie H, *et al* 2021 *ACS Nano* **15** 10444
[27] Liu Z, Guo Y, Chen Z, Gong T, Li Y, *et al*. 2022 *Nanophotonics* **11** 4409
[28] Zhang Z, You J Y, Gu B and Su G 2021 *Phys. Rev. B* **104** 174433
[29] Subhan F, Ali L, Aman R, Chen A, Peng B, *et al* 2025 *Phys. Chem. Chem. Phys.* **27** 397
[30] León A M, González J W, Mejía-López J, Crasto de Lima F and Suárez Morell E 2020 *2D Mater.* **7** 035008
[31] Jayaraman A 1983 *Rev. Mod. Phys.* **55** 65
[32] Mao H K, Xu J and Bell P M 1986 *Journal of Geophysical Research: Solid Earth* **91** 4673
[33] Ubrig N, Wang Z, Teyssier J, Taniguchi T, Watanabe K, *et al* 2020 *2D Mater.* **7** 015007
[34] Heath J J, Costa M, Buongiorno-Nardelli M and Kuroda M A 2020 *Phys. Rev. B* **101** 195439
[35] Yu T, Liu R, Mao H, Ma X, Wang G, *et al* 2022 *Phys. Rev. B* **105** 165127
[36] Wang Y, An J, Ye C, Wang X, Mai D, *et al* 2025 *Phys. Rev. Lett.* **135** 046303